The Journal of Experimental Biology 201, 573–590 (1998)
Printed in Great Britain © The Company of Biologists Limited 1998
JEB1088

THEORETICAL AND EMPIRICAL SCALING PATTERNS AND TOPOLOGICAL HOMOLOGY IN BONE TRABECULAE

SHARON M. SWARTZ*, ANTIGONE PARKER AND CHRISTINE HUO
Department of Ecology and Evolutionary Biology, Brown University, Providence, RI 02912, USA
*e-mail: sharon_swartz@brown.edu

Accepted 27 November 1997: published on WWW 26 January 1998

Summary

Trabecular or cancellous bone is a major element in the structural design of the vertebrate skeleton, but has received little attention from the perspective of the biology of scale. In this study, we investigated scaling patterns in the discrete bony elements of cancellous bone. First, we constructed two theoretical models, representative of the two extremes of realistic patterns of trabecular size changes associated with body size changes. In one, constant trabecular size (CTS), increases in cancellous bone volume with size arise through the addition of new elements of constant size. In the other model, constant trabecular geometry (CTG), the size of trabeculae increases isometrically. These models produce fundamentally different patterns of surface area and volume scaling. We then compared the models with empirical observations of scaling of trabecular dimensions in mammals ranging in mass from 4 to 40×10^6 g. Trabecular size showed little dependence on body size, approaching one of our theoretical models (CTS). This result suggests that some elements of trabecular architecture may be driven by the requirements of maintaining adequate surface area for calcium homeostasis. Additionally, we found two key consequences of this strongly negative allometry. First, the connectivity among trabecular elements is qualitatively different for small *versus* large animals; trabeculae connect primarily to cortical bone in very small animals and primarily to other trabeculae in larger animals. Second, small animals have very few trabeculae and, as a consequence, we were able to identify particular elements with a consistent position across individuals and, for some elements, across species. Finally, in order to infer the possible influence of gross differences in mechanical loading on trabecular size, we sampled trabecular dimensions extensively within Chiroptera and compared their trabecular dimensions with those of non-volant mammals. We found no systematic differences in trabecular size or scaling patterns related to locomotor mode.

Key words: trabecular bone, allometry, scaling, mammals, biomechanics.

Introduction

‘Trabeculae are not merely embodiments of mathematical abstractions; they have their own lives to lead’, J. D. Currey, *The Mechanical Adaptations of Bones*, 1984, p. 141.

Bones are complex structural entities consisting of two macroscopically distinctive tissue types: cortical or compact bone and cancellous or trabecular bone. The histology and basic biology of these bone types are similar, but they differ in their gross morphology, anatomical distribution and mechanical behavior. Cortical bone, comprising the shafts of the long bones and the outermost surfaces of all bones, is relatively stiff (elastic modulus between 17 and 25 GPa), dense and contains no visible voids (Currey, 1984). Cancellous bone, occurring in the epiphyses and metaphyses of long bones, the vertebral centra and the interior of many flat bones, consists of porous, three-dimensional networks of trabeculae, discrete plates and struts, separated by large interconnecting macroscopic spaces. The modulus of cancellous bone is considerably less than that of compact bone, varying between 0.04 and 10 GPa (Ku *et al.* 1987; Mente and Lewis, 1989; Hodgskinson and Currey, 1992; Rho *et al.* 1993), both because of the mechanical characteristics of the individual trabeculae and because of the lower apparent density (mass of bone tissue per unit bulk volume of porous bone tissue; Parfitt, 1988).

Cancellous bone is critical to the mechanical behavior of bones as organs. The intricate meshwork must transfer loads to and from cortices without undue deformation or fracture. Because of its low elastic modulus and extensive plastic deformation before failure, cancellous bone is also believed to play a critical role in absorbing the energy transmitted to joints and in attenuating joint forces, particularly during impact loading (Radin, 1982; Radin *et al.* 1970, 1973). This function depends critically on the large volume of cancellous tissue in joints, given that elastic energy absorbed in impact is a volume-dependent function (Wainwright *et al.* 1976). The large volume of trabecular bone is particularly important given its relatively low apparent density in comparison with compact bone, since

the energy absorbed by bone is proportional to apparent density and since denser bone thus absorbs more energy per unit volume (Currey, 1984). Cancellous bone is not, however, exclusively mechanical in nature. Bone also serves as the organism's primary mineral reservoir, and calcium is readily resorbed from and deposited onto the surfaces of trabeculae during normal day-to-day activities and particularly during periods of calcium stress such as pregnancy and lactation (Parfitt, 1983; Miller *et al.* 1989). Indeed, it is the cells on bone surfaces that are exposed directly to the osteoregulatory effects of prostaglandins (Jee *et al.* 1985, 1990; Mori *et al.* 1990; Lanyon, 1992*a*), suggesting that high-surface-area cancellous tissue could be particularly important in this regard.

For a given anatomical site, the spatial organization of trabeculae is non-random and often highly stereotyped. Both structural patterning and trabecular density differ from site to site within the body. Moreover, at a given anatomical site, there may be significant differences in patterns among taxa (e.g. Ward and Sussman, 1979). Variation in apparent density and architecture is believed to reflect the direction and intensity of stresses developed in bones during normal behavior (Meyer, 1867; Wolff, 1869; Lanyon, 1974; Hayes and Snyder, 1982; Goldstein, 1987). The mechanical properties of cancellous bone depend strongly on apparent density (Carter and Hayes, 1977; Goldstein, 1987; Rice *et al.* 1988; Keaveny and Hayes, 1993) and thus vary among regions within bones. Moreover, recent experimental evidence documents the sensitivity of trabecular bone modulus and strength to test specimen size and geometry (Keaveny *et al.* 1993); this suggests that the stiffness and strength of cancellous tissue in joints of diverse sizes may vary for geometric reasons alone. Presumably, then, taxa of differing body size and locomotor mode possess cancellous bone that varies in mechanical properties in correlation with body or joint size and with variation in trabecular architecture.

Within a given volume of cancellous bone, the apparent density, mechanical properties and surface area available for physiological processes are likely to depend not only on the density of trabeculae, defined in number of elements per unit volume, but also on the size of the individual elements. Stresses within individual trabeculae, and at the interconnection of trabeculae to each other and to the overlying compact bone, may also depend on the size of trabecular elements. The need to place the significance of trabecular architecture within its allometric context is particularly strong given (1) that the trabecular bone of all mammals shares a similar structural design at both gross and histological levels; (2) that joints vary in linear dimensions by over an order of magnitude within an individual; and (3) that the body size range of mammals is large (2 to 120×10^6 g; Silva and Downing, 1995). Scale effects in trabecular bone have, however, yet to be investigated. Recognizing that trabecular bone is modular in its construction, we ask how the 'modules', the individual trabeculae, scale with body size in mammals.

In this context, we have approached questions of scale in trabeculae from three perspectives. First, we explored the functional ramifications of two alternative, biologically plausible patterns by which trabecular elements might change form with changing body size: (1) constant trabecular size (CTS), in which individual trabeculae remain uniform in size and shape over all joint/body sizes; and (2) constant trabecular geometry (CTG), in which trabecular element size scales isometrically in relation to whole joint or bone size (Fig. 1). Using these two divergent patterns, we constructed theoretical models from which we derive simple predictions about changes in functional behavior of trabecular bone with scale. The differences between the CTS and CTG models provide a plausible range of variation of geometrically regular scaling in trabecular bone.

Second, we conducted an empirical scaling analysis of the dimensions of trabeculae in the limb joints of mammals ranging in body mass over five orders of magnitude. We interpret the results of this portion of the study within the context of general principles of structural allometry. In addition, these analyses tested whether trabeculae scale in the manner predicted by either the CTS or CTG models.

Third, we tested the possibility that the evolution of highly specialized limb loading regimes can lead to distinct patterns of trabecular size and scale. To do so, we separately compared the absolute size and scaling patterns of trabeculae within bats with those in non-volant mammals. We chose to sample extensively within the Chiroptera to test two specific hypotheses. First, we hypothesized that if, as proposed by previous authors, the architecture of trabecular bone is a direct reflection of the mechanical loads imposed on the tissue (Wolff, 1869; Currey, 1984; Carter, 1987; Carter *et al.* 1987; Whalen *et al.* 1988; Beaupré *et al.* 1990), then the structural design of bat humeri should differ significantly from that of bat femora. These two joint regions experience fundamentally different mechanical environments, although to date it is impossible to specify in detail the differences in mechanical loading between bat shoulder and hip joints. The humerus, including the shoulder joint, experiences very large forces and moments during both steady horizontal and turning flight, and some considerable portion of these forces must be borne by the bones themselves (Swartz *et al.* 1992; P. Watts, personal communication). In contrast, bats typically restrict their hindlimb use to head-down suspension and clambering, with some terrestrial bipedal or quadrupedal maneuvering (Vaughan, 1959). These movements probably generate axial tension and a limited amount of compression and bending. The most notable exceptions to this typical behavioral pattern are the vampire bats (Microchiroptera; subfamily Desmodontinae, genera *Desmodus*, *Diaemus* and *Diphylla*) (Altenbach, 1979). These taxa move across the ground or up and down trees with rapid, forceful jumps which, particularly in *Desmodus*, may exert significant ground reaction forces (Schutt *et al.* 1997).

In addition, we hypothesized that the forces experienced by both bat forelimb and hindlimb joints differ from those of non-volant mammals. The magnitude of compressive forces is certainly far less in both sets of bat limb joints, although torsion may be greater in bat humeri (Swartz *et al.* 1992). Although it is difficult to predict *a priori* how the details of trabecular

architecture should differ under these distinctive loading regimes, we predict that if mechanical usage dictates structural design then the trabecular bone of volant and non-volant mammals should differ significantly in structure.

Materials and methods

Modeling changing geometries in regular trabecular arrays

Our models emphasize the modular nature of trabecular bone: each organ of trabecular bone, or 'joint', contains elements of similar geometry interconnected to one another to form a regular network of support elements. We model 'joints' as cubic volumes; in the constant trabecular size (CTS) model, each joint is composed of multiple repeating constituent cubic subunits, while in the constant trabecular geometry (CTG) model, a single subunit varies in size (Fig. 1). In each model, the total size of the cube represents that of the abstracted joint or epiphyseal region and is filled with trabecular structures. The empty space between trabeculae represents the marrow spaces. The total size of each joint cube increases in successive iterations of the model, and increasing joint size represents proportional increases in body size. The dimensions of the trabecular elements of the smallest subunit in the CTG model and all trabeculae of the CTS model are based on realistic dimensions of mammalian trabeculae, as determined in the empirical scaling portion of this study.

We selected simple cubic shapes to represent joint regions rather than more anatomically realistic geometries because cubic volumes (1) facilitate packing of regularly spaced trabecular elements into each defined volumes, (2) allow modeling of a modular design comprising repeats of single, simple cubic volumes, (3) are readily modeled over a range of sizes, and (4) produce element packing which is a reasonable first approximation of the distribution of trabeculae in bone tissue (Fig. 1). Moreover, although our model does not account for the presence of plate-shaped trabeculae, actual rod-shaped trabecular elements are cylindrical in overall shape, approximately the same length within a given joint and linear rather than curved; they can therefore be reasonably approximated as rectangular beams of uniform size. Moreover, within any joint subregion, trabeculae are packed at relatively uniform densities, although the apparent density of trabecular bone varies regionally within large and complex joints (Whitehouse, 1974; Hayes and Snyder, 1982; Goldstein, 1987; Keaveny and Hayes, 1993). Cubic volumes packed with mutually perpendicular trabeculae thus represent a realistic and tractable abstraction of the naturally occurring architecture of cancellous bone tissue.

In both the CTS and CTG models, the trabecular architecture of the subunits is created by the assembly of repeats of two geometric elements – rectangular prism-shaped *struts*, arrayed along the mutually perpendicular edges of the cubic multi- and subunit edges, and *interconnection cubes*, located at the corners where struts intersect (Fig. 1). The role of the interconnection cubes is to facilitate trabecular packing and to connect the struts. Structurally, the interconnection cubes are continuous with the struts and represent a portion of each strut to which they connect, rather than discrete entities. They are treated as elements distinct from the struts only to facilitate computation of surface area and volume changes with overall size. The two models differ in how trabecular structure changes with increments of increasing size or size factor (see below). The external dimensions of the cube enclosing the trabecular columns represent an estimate of the joint size. At a given size factor, the external cube or abstract joint is identical in the CTS and the CTG models. From the two models, we calculated nine numerical surface area and volume parameters for each iteration of the model (Table 1).

To increase the size of the theoretical joints of the CTS model in each successive iteration, *n*, struts and interconnection cubes are added to create new, larger networks of consistently arranged elements. The dimensions of the trabecular elements are an idealization based on the empirical data presented in the

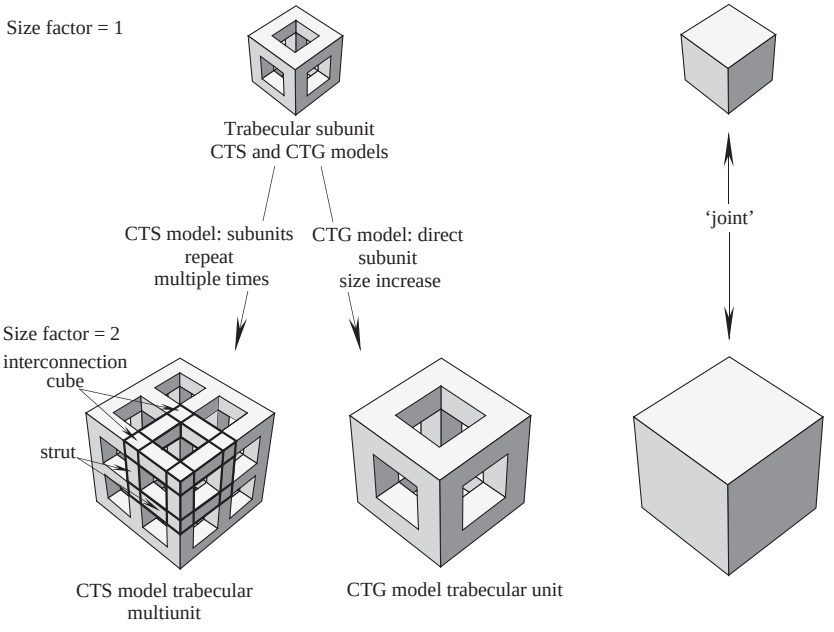

Fig. 1. Schematic geometry of the constant trabecular size (CTS) and constant trabecular geometry (CTG) models. Each trabecular subunit is represented as a rectangular column packed into a cubic array. At a size factor of 1, the CTS and CTG models are identical and are composed of a single unit. These trabeculae can be envisioned as filling a cubic 'joint' of the same external dimensions as the trabecular subunit. As size increases in successive iterations of the model, the two models diverge in architecture. At a size factor of 2, size increase is accomplished in the CTS model *via* addition of new subunit structures into a larger multiunit (left). In the CTG model, the increase from size factor 1 to size factor 2 occurs by a proportional increase in size of all trabecular edge elements of the subunit structure.

Table 1. *Parameters calculated in the CTS and CTG models*

Parameter	
n_t	Total number of trabeculae
A_t	Total trabecular surface area
V_t	Total trabecular volume
A_j	Total joint surface area
A_t/V_t	$\frac{\text{Total trabecular surface area}}{\text{Total trabecular volume}}$
V_j	Total joint volume
A_j/V_j	$\frac{\text{Total joint surface area}}{\text{Total joint volume}}$
A_t/A_j	$\frac{\text{Total trabecular surface area}}{\text{Total joint surface area}}$
V_t/V_j	$\frac{\text{Total trabecular volume}}{\text{Total joint volume}}$

Each of these values was calculated for joints ranging in size from a single subunit to a multiunit of 240 subunits × 240 subunits × 240 subunits, a 200-fold increase in size.

The absolute size of the largest joint is 12.01 cm × 12.01 cm × 12.01 cm, typical of a large joint such as the femoral head in a large-bodied mammal.

allometric analysis portion of this study: mean trabecular length is taken as 0.400 mm and mean diameter as 0.100 mm. Each size increase is implemented by the addition of enough trabecular elements to create additional cubic subunits rather than a duplication of the original complete subunit; addition of entire subunits stacked upon one another would create struts of double thickness along the edges where two adjacent subunits contact one another. The newly packed subunits created by additional trabecular elements with each iteration form the components of larger cubes, or multiunits (Fig. 1). All multiunits are cubic in overall shape. Because complete subunits are not duplicated in the successive iterations by which the model grows in size, iterations do not represent integral increases in the length of an edge of the CTS multiunit or CTG unit, but instead are increases by a size factor k (see below and Appendix).

In the CTG model, the trabecular elements of the single smallest subunit are the sole supports for the structure throughout increases in size. Trabecular element number and geometry thus remain constant while the absolute size of the elements increases progressively with each iteration of the model (Fig. 1). For any iteration, the length and diameter of each trabecular element and the total length of the joint are increased at the same rate. We determined the proportional increase for each iteration by calculating a size factor k. This size factor adjusts the growing length and diameters of the CTG trabecular elements so that total CTG unit size always equals total CTS multiunit size. With each successive model iteration n, we multiplied the length and diameter of the CTG trabecular elements by k. For the second iteration of the model, for example, k=1.83, resulting in slightly less than a doubling of edge length. The formulae describing k and the model surface area and volume parameters for both models are given in the Appendix. The multiunits range in size from a single cubic subunit to 240×240×240 subunits. Because each subunit after the first in the CTS model is smaller than the initial complete subunit, to avoid duplications of struts at edges where new subunits are added (see above), the largest joint is approximately 200 times the length of the smallest. Its absolute size is 12.01 cm×12.01 cm×12.01 cm, a reasonable estimate of the size of a large joint such as the femoral head in a very large-bodied mammal.

Curve fitting

For each model, linear or power functions, as appropriate, were used to fit curves describing changes in surface area or volume parameters in relation to overall joint/body size. In most cases, it was possible to fit curves using Pearson product moment correlations of r=1.00 (equations are given in Table 2). In cases where such curve fits were not possible, we have not specified the curve of the closest fit since it does not describe the algebra of the underlying relationship.

Allometric analysis sample

We measured the length and mid-element diameter of a number of trabeculae from humeral and femoral heads of a variety of small, medium-sized and large mammals, including a diversity of bats and of non-volant mammals (Table 3). We sampled bat trabecular bone from taxa ranging in body mass from 5 to 700 g, drawn from both bat suborders (Microchiroptera and

Table 2. *Linear, power or polynomial functions (*y*), used as appropriate to fit curves describing changes in surface area or volume parameters with size factor (*x*) for the CTS and CTG models (Figs 3, 4)*

Parameter	CTG model	CTS model
A_t	$y=2.16\times10^{6}x^{2.00}$	$y=1.15\times10^{6}x^{2.93}$
$\frac{A_t}{A_j}$	$y=1.00$	$y=0.38x+0.51$
V_t	$y=5.60\times10^{7}x^{3.00}$	$y=3.07\times10^{7}x^{2.94}$
$\frac{V_t}{V_j}$	$y=0.26$	Interpolated
$\frac{A_t}{V_t}$	$y=8.86\times10^{-2}x^{-1.00}$	Interpolated
$\frac{\left(\frac{A_t}{V_t}\right)}{\left(\frac{A_j}{V_j}\right)}$	$y=3.86$	$y=3.69x+0.15$
$\frac{\left(\frac{A_t}{V_t}\right)_{CTS}}{\left(\frac{A_t}{V_t}\right)_{CTG}}$	$y=0.96x+0.039$	

In all cases in which curves were fitted, Pearson product moment correlations (*r)* were equal to 1.00 and P values were $\leqslant$0.0001.

Megachiroptera) and several families (Table 3). Samples were either taken from freshly frozen material collected and made available to us by field workers sampling bats for other studies or were prepared from alcohol-preserved material loaned from the collections of the American Museum of Natural History.

Our sample of non-volant mammals was collected opportunistically from specimens readily available in our laboratories and includes marsupials, insectivores, rodents, primates, lagomorphs, carnivores, perissodactyls and cetaceans. This sample was constructed to sample as broad a range of body sizes as possible. In all cases, animals were skeletally mature, as indicated by epiphyseal fusion, and in apparently good health, with no signs of limb or skeletal deformities of any kind.

We selected the proximal femur and humerus as the foci of our analysis. Analysis and discussion of trabecular bone architecture has often centered on the femoral head and neck, going back to the original formulation of Wolff's Law (Wolff, 1869; Whitehouse and Dyson, 1974; Lanyon and Rubin, 1985; Carter *et al*. 1987). Our use of this anatomical region permitted us to compare our results with those of previous workers interested in the dimensions of individual trabeculae (Whitehouse, 1974, 1975; Whitehouse and Dyson, 1974). Furthermore, the organization of individual trabeculae into tracts of highly oriented elements is very clear in the proximal femur. We include the humeral head to compare forelimb and hindlimb scaling patterns and to determine whether scaling patterns are uniform throughout the body.

To assess trabecular structure, we sectioned each bone just distal to the proximal epiphyseal trabeculae, and cleaned and removed marrow and fat using a combination of incubation in antiformin solution (Green, 1934) and ultrasonication. We then mounted our specimens with the intact joint surface embedded in modeling clay, with the cut surface upwards (Fig. 2); when necessary, we used a small hand drill to remove cortical bone remaining distal to the region of trabeculae. We used macrophotography, photomicroscopy of whole mounts viewed using a dissecting microscope (Leica WILD M420 dissecting microscope with a PAC Hund Wetzlar attachment for a Ricoh camera) or scanning electron microscopy (Hitachi S-2700) to capture standardized, scaled images of the distalmost trabeculae in each joint. Visual inspections of trabeculae from deeper regions of the joints show no regular patterns of change in trabecular size with depth. We consider the distalmost trabeculae, readily accessible using this technique without causing damage to other portions of the trabecular network, to be representative of those throughout the joint region. By

Table 3. *Species used for analysis of trabecular size and scaling*

Bats			Non-volant mammals		
Species	Family	Body mass, g (N_I, $N_{T\text{-}H}$, $N_{T\text{-}F}$)	Species	Order	Body mass, g (N_I, $N_{T\text{-}H}$, $N_{T\text{-}F}$)
Myotis lucifugus	Vespertilionidae	4.6 (5,32, 26)	*Sorex cinereus*	Insectivora	4 (2, 3, 2)
Natalus tumidirostris	Natalidae	7 (1,5,4)	*Cryptotis parva*	Insectivora	5.5 (1, 5, 3)
Rhinolophus stheno	Rhinolophidae	7.9 (2, 8, –)	*Reithrodontomys megalotis*	Rodentia	14 (1, –, 2)
Saccopteryx bilineata	Emballonuridae	8 (2, –, 8)	*Glaucomys volans*	Rodentia	115 (1, 3, 4)
Peropteryx kappleri	Emballonuridae	9.6 (1, 8, 3)	*Tamiasciurus hudsonicus*	Rodentia	225 (1, 4, 3)
Molossus molossus	Molossidae	10.1 (2, 6, 4)	*Sciurus carolinensis*	Rodentia	600 (2, 7, 6)
Tadarida brasiliensis	Vespertilionidae	12.5 (2, 3, 7)	*Potorous tridactylus*	Marsupialia	1000 (2, 6, 8)
Miniopterus australis	Vespertilionidae	13 (2, 7, –)	*Oryctolagus cuniculus*	Lagomorpha	3500 (2, 7, –)
Pteronotus parnellii	Mormoopidae	15 (3, 16, 12)	*Macropus eugenii*	Marsupialia	4000 (1, 4, 4)
Carollia perspicillata	Phyllostomidae	15 (1, 6, –)	*Cercopithecus* sp.	Primates	5100 (1, 4, 4)
Vampyrops helleri	Phyllostomidae	15.4 (1, 3, –)	*Macaca fascicularis*	Primates	5200 (2, 8, 8)
Macrotus waterhousii	Phyllostomidae	16 (1, 6, –)	*Hylobates lar*	Primates	5900 (1, 5, 5)
Uroderma bilobatum	Phyllostomidae	17 (1, 6, –)	*Macaca arctoides*	Primates	10 000 (1, 7, –)
Lasiurus cinereus	Vespertilionidae	18 (1, 6, –)	*Canis familiaris*	Carnivora	23 000 (2, 6, 8)
Lasiurus borealis	Vespertilionidae	18 (1, –, 4)	*Homo sapiens*	Primates	65 000 (3, 15, 10)
Eptesicus fuscus	Vespertilionidae	22 (4, 17, 25)	*Equus caballus*	Perissodactyla	530 000 (2, –, 28)
Diphylla ecaudata	Phyllostomidae	28 (3, 11, 5)	*Megaptera novaeangliae*	Cetacea	40 000 000 (1, 19, –)
Syconycteris australis	Pteropodidae	30 (2, 10, 6)			
Desmodus rotundus	Phyllostomidae	33 (3, 12, 11)			
Hipposideros diadema	Hipposideridae	36.2 (3, 10,12)			
Diaemus youngi	Phyllostomidae	38 (3, 12, 8)			
Cynopterus sphinx	Pteropodidae	40.6 (2, 7, 7)			
Artibeus jamaicensis	Phyllostomidae	65.5 (1, 5, –)			
Phyllostomus hastatus	Phyllostomidae	75 (2, –, 12)			
Pteropus poliocephalus	Pteropodidae	700 (3, 16, 7)			

For individuals without directly associated body mass data, species mean values were taken from the literature (Nowak, 1991; Silva and Downing, 1995).

N_I is the number of individuals sampled, $N_{T\text{-}H}$ is the number of humeral trabeculae and $N_{T\text{-}F}$ is the number of femoral trabeculae.

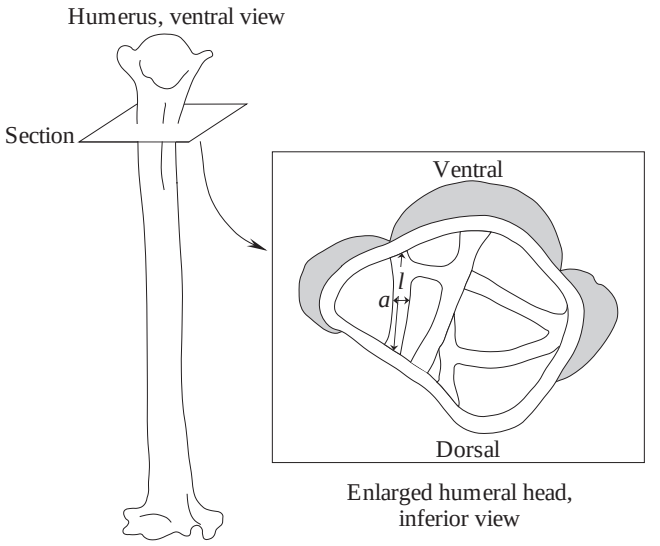

Fig. 2. Sample preparation technique for empirical scaling studies. Each humerus or femur was sectioned transversely just distal to the joint region, then positioned to allow viewing of the interior of the epiphysis. *l*, total length of trabecula; *a*, mid-element diameter of trabecula.

sampling only from the planes closest to the plane of section, we minimize parallax as a source of measurement error. From enlargements of each photograph or photomicrograph, we measured the total length *l* and mid-element diameter *a* from all trabeculae that could be viewed in their entirety and were parallel to the plane of the image (between three and 10 elements from each specimen). In all, we sampled 489 trabeculae from 66 individuals of 42 species (see Table 3).

Statistical analyses

To improve normality of distribution and to facilitate allometric analysis, all measurements were log-transformed before statistical analysis. We used ordinary least-squares linear regression (OLS) to describe the relationships between trabecular dimensions and body mass. Body mass measurements were the *pre-mortem* masses of each individual whenever possible; when direct body mass measurements were not available, we used species means from the literature (Nowak, 1991; Silva and Downing, 1995). We used analysis of covariance (ANCOVA) to compare regressions among groups or bones when regression slopes for the two did not differ significantly; when slopes differed, we used Tsutakawa's quick test for comparisons of elevations with differing slopes (Tsutakawa and Hewett, 1977). In addition, we performed statistical analyses on species means to compare with our results from the complete data set.

Results

Trabecular surface area and volume in CTS and CTG models

Trabecular surface area (A_t) increases with increasing body size in both the CTS and CTG models; A_t values are similar in the two models at small sizes, but since A_t increases far more rapidly in the CTS model, in proportion to (size factor)$^{2.93}$, than in the CTG model, in proportion to (size factor)$^{2.00}$, the two models rapidly diverge. The two models differ in surface area by an order of magnitude by size factor 30 (joint size approximately 18 mm edge length) (Fig. 3A; Table 2). At the largest size modeled, trabecular surface area is approximately 80 times greater in the CTS than in the CTG model.

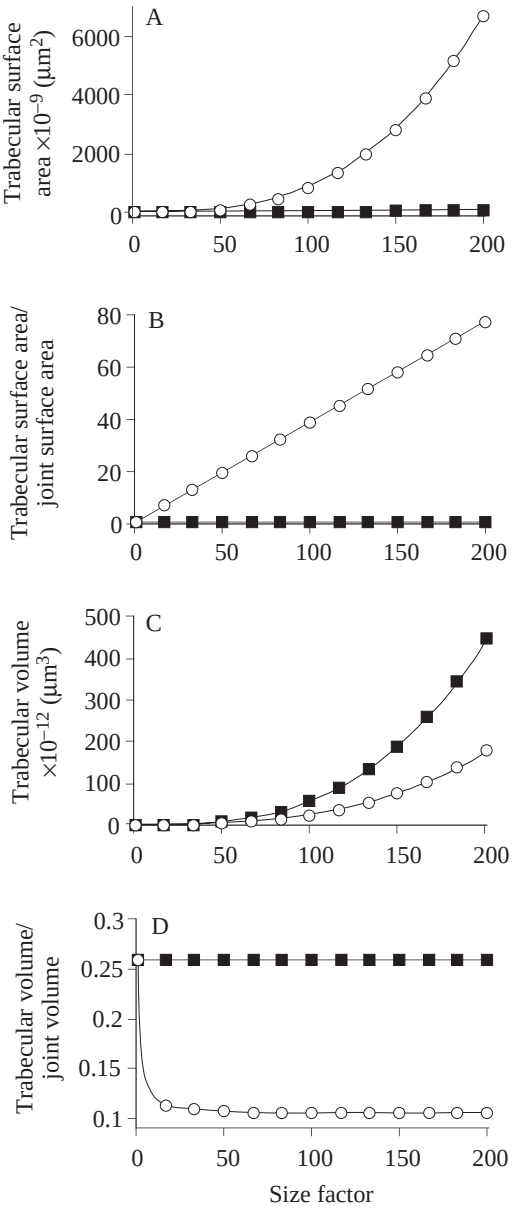

Fig. 3. Change in surface area and volume variables with size factor. Values derived from the CTS model are indicated as open circles; those derived from the CTG model are filled squares. The equations describing these lines are given in Table 2.

The ratio of A_t to the total surface area of the joint (A_j) gives a measure of the amount of trabecular surface available for metabolic processes relative to a rough estimate of the weight-bearing capacity of the joint. In the CTS model, A_t/A_j increases

linearly with increasing size (Fig. 3B; Table 2). In the CTG model, where increase in size is achieved by an increase in trabecular dimensions in proportion to the changing total joint size, A_t/A_j is 1.00 and does not change as size factor increases (Fig. 3B; Table 2). This ratio will be constant for any CTG model and is equal to 1.0 because of the specific dimensions assigned here to the trabeculae relative to the joint.

In contrast to the pattern for surface areas, the volume of trabecular bone, V_t, increases more rapidly with joint size in the CTG model than in the CTS model (Fig. 3C; Table 2). By a size factor of 5, equivalent to a cube with a 3.1 mm edge, the trabecular volume in the CTG model is double that of the CTS model. Although the two models continue to diverge, they do so slowly such that, when size factor reaches 200, the two differ by a factor of approximately 2.5. In the CTS model, the ratio of V_t (trabecular volume) to V_j (total joint volume) decreases steeply at small sizes, and then levels out asymptotically with increasing size factor (Fig. 3D; Table 2). The V_t/V_j ratio of the CTG model, however, remains constant.

The surface area to volume ratio of trabecular bone, A_t/V_t, is nearly constant in the CTS model (Table 2) because each new trabecular volume increment arises through the addition of new trabeculae of constant surface area (Fig. 4A). In the CTG model, however, A_t/V_t decreases rapidly, as new volume and surface area increments are added *via* size increases of the original 12 trabeculae; this change in surface area relative to volume approaches that of the entire joint (Fig. 4A). The two models are identical at a size factor of 1, differ by an order of magnitude at a size factor of 13 (edge length 6.6 mm) and differ almost 200-fold at a size factor of 200.

The CTS model A_t/V_t increases rapidly relative to the surface area/volume ratio for the joint; it is 10 times greater than A_j/V_j at a size factor of 3 (edge length 1.6 mm), 100 times greater at a size factor of 28 (edge length 16.6 mm) and 750 times greater than A_j/V_j at a size factor of 200 (Fig. 4B; Table 2). At these same sizes, A_t/V_t is, respectively, 2.6, 27 and 191 times greater for the CTS model than for the CTG model. The rate of A_t/V_t decrease for the CTG model is the same as the rate of surface area/volume decrease for the joint as a whole, although the absolute ratio is 3.86 times higher for the trabecular geometry than for a solid cube (Fig. 4B; Table 2).

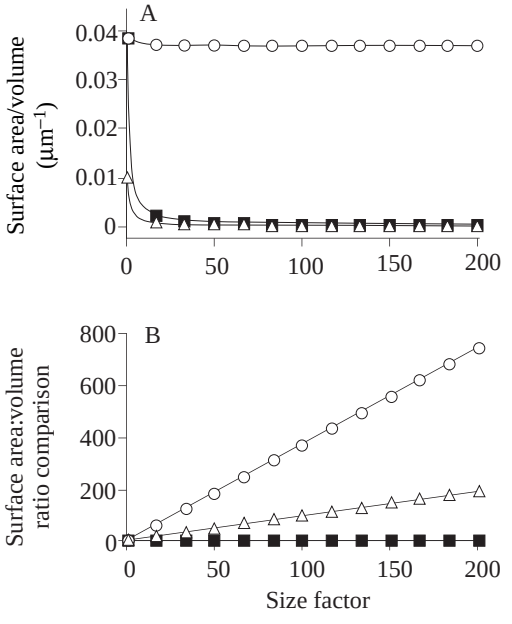

Fig. 4. Change in trabecular surface area/volume ratio (A) and the ratios of surface area/volume of the two models relative to one another and to the joint (B). (A) CTS model, open circles; CTG model, filled squares; total joint, open triangles. (B) CTS model/total joint, open circles; CTG model/total joint, filled squares; CTS/CTG, open triangles.

Trabecular dimension scaling: empirical results

Within each joint of each individual, trabeculae vary somewhat in length and diameter (Fig. 5; Table 4). This variation within each individual has an important influence on our scaling analyses, resulting in considerable scatter in the data at all body sizes. This scatter reflects the natural variation in trabecular size within any joint rather than measurement error, so we have elected to retain this variation in our subsequent analyses. We also separately analyze the mean values of trabecular dimensions for each species.

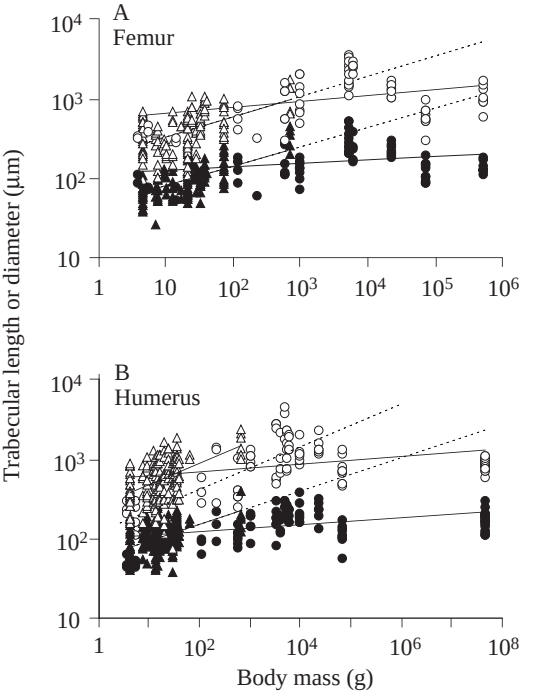

Fig. 5. Double-logarithmic plot of trabecular length or diameter with respect to body mass for bats and non-volant mammals for the femur (A) and humerus (B). Multiple trabeculae from each individual are plotted to indicate the range of within-individual variation in trabecular dimensions; each symbol represents a single trabecula. Lengths are represented by open symbols, diameters by filled symbols; bats are represented by triangles, and non-volant mammals by circles. Continuations of regression lines for bats are indicated as dotted lines. Regression statistics for these data are given in Table 5.

Scaling coefficients for double-logarithmic regressions of trabecular dimensions *versus* body mass for all mammalian taxa examined together were all lower than 0.17, and most were below 0.10 (Table 5); values of 0.33 would indicate isometric scaling. For both trabecular length and diameter, this negative allometry is also indicated by the broadly overlapping range of values for the very smallest and very largest taxa in our sample (see Table 4): there is little difference in absolute trabecular size even when the extremes of the body size range sampled are compared (Fig. 5). Our results also indicate negative allometric scaling among non-volant mammals, with coefficients ranging between 0.044 and 0.186. Scaling patterns calculated from the entire sample did not differ significantly from those calculated from species mean values (Table 5).

The scaling relationships for trabeculae from bats differed from the overall mammalian pattern. The scaling coefficients were generally higher and approached isometry; they varied from 0.202 to 0.326 (Table 5). Indeed, when species means were used in the statistical analyses, we found isometry to define the scaling relationship for trabecular length in both the humerus and the femur, and for trabecular diameter in the femur. When the variation of all the data points was retained, isometry was found only in the trabecular length in the humerus.

Within bats (Fig. 6), and within non-volant mammals, regression slopes did not differ significantly between the humerus and the femur, despite the prediction that extreme differences in mechanical loading of the hip and shoulder joints would lead to differences in trabecular structure in bats. Moreover, vampire bats were statistically indistinguishable from the remaining bat taxa, with no evidence of any trabecular hypertrophy correlated with significantly increased loading of the hindlimbs in comparison with their relatives.

Comparisons of bats and non-volant mammals

We found some distinct differences between locomotor groups in trabecular size (Fig. 5). ANCOVA showed that regression slopes differed significantly between groups for both femoral trabecular length and diameter ($P<0.05$), with regression slopes uniformly steeper for bats than for the non-volant mammals. When species means were used, however, the regression slopes of bats and non-volant mammals differed only for femur trabecular diameter. Because group slopes differed statistically, conventional ANCOVA was not appropriate for comparisons of elevations. Tsutakawa's quick test showed that elevations were not significantly different between bats and non-volant mammals for the femur (length, $\chi^2=0.1116$, $P=0.7383$, d.f.=1; diameter, $\chi^2=0.6523$, $P=0.4193$,

Table 4. *Within-species variation in trabecular dimensions for the humerus and femur*

	Humerus					Femur				
	N_I, $N_{T\text{-}H}$	Mean length	CV	Mean diameter	CV	$N_{T\text{-}F}$	Mean length	CV	Mean diameter	CV
Interspecific comparisons										
Bats										
Myotis lucifugus	5, 32	567.7	0.62	77.7	0.40	26	388.8	0.41	86.3	0.69
Natalus tumidirostris	1, 5	593.6	0.48	80.5	0.52	4	315.9	0.15	55.5	0.38
Rhinolophus stheno	2, 8	485.6	0.46	91.0	0.28	0				
Saccopteryx bilineata	2, 0					8	223.2	0.61	67.4	0.27
Peropteryx kappleri	1, 8	517.8	0.52	120.0	0.34	3	260.7	0.14	116.5	0.11
Molossus molossus	2, 6	421.7	0.52	112.4	0.34	4	200.4	0.18	75.8	0.23
Tadarida brasiliensis	2, 3	887.2	0.33	108.3	0.21	7	361.1	0.58	81.8	0.42
Miniopterus australis	2, 7	577.3	0.45	101.0	0.25	0				
Pteronotus parnellii	3, 16	482.4	0.57	77.7	0.40	12	483.5	0.45	95.1	0.55
Carollia perspicillata	1, 6	502.7	0.40	124.4	0.28	0				
Vampyrops helleri	1, 3	675.0	0.56	153.8	0.65	0				
Macrotus waterhousii	1, 6	526.4	0.62	172.3	0.28	0				
Uroderma bilobatum	1, 6	499.7	0.24	102.9	0.44	0				
Lasiurus cinereus	1, 6	701.0	0.56	106.9	0.20	0				
Lasiurus borealis	1, 0	613.2	0.69	108.9	0.25	4	445.2	0.10	116.5	0.11
Eptesicus fuscus	4, 17	567.7	0.72	112.5	0.25	25	338.6	0.50	85.0	0.44
Diphylla ecaudata	3, 11	810.9	0.45	113.3	0.32	5	723.0	0.30	130.3	0.21
Syconycteris australis	2, 10	501.0	0.45	72.4	0.33	6	289.2	0.32	104.0	0.23
Desmodus rotundus	3, 12	719.9	0.27	132.7	0.20	11	502.1	0.24	84.9	0.24
Hipposideros diadema	3, 10	865.3	0.60	154.2	0.25	12	425.8	0.28	75.8	0.65
Diaemus youngi	3, 12	667.3	0.35	126.1	0.31	8	824.7	0.18	123.3	0.23
Cynopterus sphinx	2, 7	617.0	0.45	112.3	0.14	7	905.8	0.23	75.8	0.31
Artibeus jamaicensis	1, 5	1065.9	0.09	158.5	0.09	0				
Phyllostomus hastatus	2, 0					12	556.5	0.41	146.8	0.40
Pteropus poliocephalus	3, 16	1628.4	0.35	200.4	0.49	7				

d.f.=1); for the humerus, bats showed significantly longer trabeculae (Tsutakawa's quick test, length, χ^2=4.816, *P*=0.0282, d.f.=1; diameter, χ^2=0.9050, *P*=0.3415, d.f.=1). To test the possibility that differences in trabecular scaling between groups were related to differences in whole-bone size at comparable body sizes, we also carried out ANCOVAs of trabecular dimensions in relation to midshaft bone diameters and bone lengths. These results were identical to those derived from the body mass data.

For non-volant mammals, the slope of trabecular length *versus* trabecular diameter did not differ significantly from 1.00 (Table 6; Fig. 7); the shape of individual trabeculae is, on average, invariant in relation to body mass. In contrast, the aspect ratio of trabeculae in bats did vary with body mass, with the slope of the trabecular length *versus* trabecular diameter regressions being significantly less than 1.00 for both the femoral and humeral heads. Thus, larger bats have absolutely shorter trabeculae for a given diameter than comparably sized non-volant mammals and relatively shorter trabeculae in relation to diameter than small bats. Within bats, the aspect ratios of vampire bat trabeculae were not statistically distinguishable from those of bat species that do not adopt extreme jumping and climbing behaviors (Fig. 7).

Discussion

Scaling of surface area and volume

The relationship between surface area and volume is fundamental to function, development and, indeed, almost all aspects of the design of organisms and their constituent organs,

Table 4. *Continued*

	Humerus					Femur				
	N_I, $N_{T\text{-}H}$	Mean length	CV	Mean diameter	CV	$N_{T\text{-}F}$	Mean length	CV	Mean diameter	CV
Interspecific comparisons										
Non-volant mammals										
Sorex cinereus	2, 3	243.6	0.19	51.7	0.18	2	329.6	0.03	98.0	0.16
Cryptotis parva	1, 5	192.9	0.41	49.0	0.09	3	419.5	0.11	75.9	0.03
Reithrodontomys megalotis	1, 0					2	299.9	0.08	65.2	0.26
Glaucomys volans	1, 3	421.7	0.36	86.0	0.24	4	643.0	0.29	140.0	0.31
Tamiasciurus hudsonicus	1, 4	1019.0	0.63	51.7	0.18	3	320.4	0.24	61.3	0.13
Sciurus carolinensis	2, 7	452.1	0.60	109.3	0.24	6	916.4	0.55	175.7	0.44
Potorous tridactylus	2, 6	1010.0	0.19	162.8	0.29	8	1183.4	0.52	131.8	0.26
Oryctolagus cuniculus	2, 7	1783.9	0.65	182.8	0.37	0				
Macropus eugenii	1, 4	1163.6	0.57	153.2	0.23	4	535.4	0.45	105.2	0.35
Cercopithecus sp.	1, 4	3446.3	0.43	289.0	0.11	4	2486.0	0.35	245.7	0.33
Macaca fascicularis	2, 8	1526.6	0.44	219.0	0.14	8	1974.0	0.41	347.8	0.36
Hylobates lar	1, 5	1641.2	0.20	196.0	0.18	5	2554.0	0.14	239.2	0.36
Macaca arctoides	1, 7	1230.1	0.30	222.6	0.37	0				
Canis familiaris	2, 6	1500.3	0.28	238.1	0.29	8	1313.9	0.18	234.5	0.18
Homo sapiens	3, 15	765.2	0.38	117.7	0.28	10	612.4	0.30	125.0	0.28
Equus caballus	2, 0					28	1137.4	0.33	140.1	0.16
Megaptera novaeangliae	1, 19	894.0	0.15	176.5	0.26	0				
Intraspecific comparisons										
Eptesicus fuscus		626.0	0.87	105.8	0.29		292.3	0.51	107.6	0.42
		511.5	0.76	112.5	0.29		400.8	0.44	69.2	0.34
		568.4	0.71	111.8	0.21		325.8	0.50	82.4	0.40
		565.2	0.56	120.3	0.20		340.5	0.56	68.2	0.20
Myotis lucifugus		432.8	0.61	72.7	0.33		451.9	0.23	107.4	0.91
		456.2	0.50	81.5	0.49		340.5	0.55	62.0	0.37
		309.2	0.37	50.8	0.15		356.9	0.49	69.4	0.49
		654.8	0.55	76.4	0.24		395.4	0.35	80.5	0.55
		484.4	0.47	93.3	0.44		379.9	0.48	93.0	0.44

Coefficients of variation (CV) are calculated as standard deviation/mean.
For some taxa, data are available for the humerus or femur only.
All measurements are in μm.
Species are listed in order of increasing body mass and for bats and non-volant mammals separately.
N_I is the number of individuals sampled in each species, $N_{T\text{-}H}$ is the number of humeral trabeculae and $N_{T\text{-}F}$ is the number of femoral trabeculae.
Species average values are followed by individual means and coefficients of variation for several individuals of two representative species.

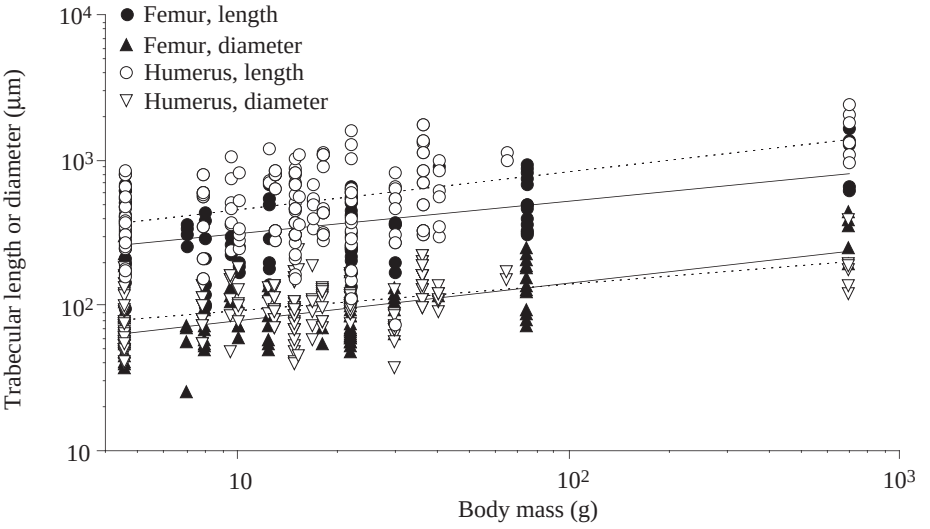

Fig. 6. Double-logarithmic plot of trabecular length and diameter with respect to body mass for the femur and the humerus of bats. Each point represents a separate trabecula. Solid lines indicate regression lines for the femur, dashed lines for the humerus. There were no statistically significant differences in the slopes for the trabeculae from the two bones.

tissues, cells and organelles. Processes through which structures relate to their external surroundings are functions of surface areas, while many internal processes and functional capabilities depend primarily on mass, volume or volume-related parameters. In the absence of size-dependent shape changes, surface areas increase in proportion to the square of a structure's linear dimensions while volumes are proportional to cube of the linear dimensions. Hence, reorganization of structural geometry is required to maintain constant surface area to volume ratios over a significant size range. In contrast, the more common relationship in the biological world is changes in surface area to volume relationships in concert with changes in organismal size and scale change; for example, gill surface areas increase in proportion to (body mass)$^{0.85–0.90}$ (Muir and Hughes, 1969).

Effect of alternative scaling regimes: modeling results

Whole bones, viewed as beam-like structures, have mechanical capabilities that vary with size (e.g. Alexander *et al.* 1979; Prange *et al.* 1979; Biewener, 1983; Economos, 1983; Steudel and Beattie, 1994). The structural design of trabecular bone has not previously been viewed from a scaling perspective, but the results of both the CTS and CTG models emphasize the importance of size to our understanding of the biology of cancellous tissue. Both models entail strong size-dependence of some functionally important features of cancellous bone. This implies that the mechanical and physiological capacities of trabecular bone vary with body size and, indeed, joint size whether CTS, CTG or some intermediate alternative best describes the size-related pattern of cancellous architecture.

The CTS and CTG models of trabecular scaling produce fundamentally different patterns of available surface area and volume as body or joint size changes. Although the two models differ little for small joints, particularly those smaller than 1 cm^3, geometric changes alone produce increasingly different

Table 5. *Results of regression analysis of log(trabecular dimensions)* versus *log(body mass)*

		Total sample[a]		Non-volant mammals[b]		Bats[c]	
		Slope	r^2	Slope	r^2	Slope	r^2
Complete data set							
Femur	Length	0.151±0.013	0.411	0.075±0.026	0.116	0.243±0.041	0.215
(N=256[a], 95[b], 161[c])	Diameter	0.098±0.010	0.328	0.044±0.019	0.074	0.257±0.031	0.352
Humerus	Length	0.076±0.009	0.207	0.050±0.015	0.205	0.292±0.048*	0.161
(N=315[a], 103[b], 212[c])	Diameter	0.058±0.006	0.290	0.048±0.010	0.288	0.202±0.028	0.215
Species averages							
Femur	Length	0.166±0.030	0.545	0.136±0.047	0.437	0.326±0.084*	0.539
(N=30[a], 14[b], 16[c])	Diameter	0.106±0.023	0.456	0.087±0.035	0.357	0.309±0.050*	0.747
Humerus	Length	0.118±0.025	0.536	0.186±0.042	0.630	0.326±0.083*	0.435
(N=38[a], 15[b], 23[c])	Diameter	0.116±0.045	0.503	0.090±0.028	0.546	0.163±0.046	0.387

Slopes are reported ± S.E.M.; all are significant at P≤0.0001. All slopes are significantly greater than zero. Slopes that are not significantly less than 0.33 are indicated with an asterisk. In no cases do the slopes for the humerus *versus* femur differ significantly.

Table 6. *Results of regression analysis of trabecular length* versus *diameter*

	Total sample[a]		Non-volant mammals[b]		Bats[c]	
	Slope	r^2	Slope	r^2	Slope	r^2
Femur (N=256[a], 95[b], 161[c])	0.972±0.069	0.509	1.080±0.102	0.635	0.596±0.092*	0.248
Humerus (N=315[a], 103[b], 212[c])	0.903±0.070	0.385	0.984±0.123	0.507	0.682±0.090*	0.230

Slopes significantly different from 1.00 are indicated with an asterisk.
All $P \leqslant 0.0001$ for all regressions.

surface area and volume relationships for the two scaling alternatives. With increasing size, trabecular surface area increases far more rapidly in the CTS than in the CTG model. In a joint the size of a typical human femoral or humeral head, the CTS model would give a trabecular surface area of close to 0.5 m^2; for the largest joints modeled here, approximately the size of the femoral head of a large horse, the trabecular surface area within the joint is over 6 m^2. In contrast, trabecular volumes increase disproportionately with size in the CTG model. While the divergence in trabecular volumes of the two models is less drastic than that of trabecular surface areas, the difference at large body sizes still has the potential to be functionally significant. In comparison with CTS scaling, if CTG scaling were the rule, a large joint in a large-bodied mammal would have 2.5 times the cancellous bone tissue to build and maintain or, viewed somewhat differently, 2.5 times the tissue available for distributing joint forces.

In trabecular bone, quite distinct phenomena are dictated by available surface area *versus* volume or mass. For example, total body mineral homeostasis requires the release of calcium from bone surfaces and its deposition onto those same surfaces. Surface areas may need to keep pace with the mass of tissue maintained metabolically; basic physiological processes may require large animals or joints to have a disproportionately large free trabecular surface area. The large surface areas available within the cancellous tissue suggest that this is a critical locus of metabolic calcium mobilization (Kaplan *et al.* 1994). In one estimate, it has been hypothesized that trabecular bone is responsible for approximately 70 % of the total calcium turnover per day (Parfitt, 1983); this estimate, however, does not account for the differences in design among animals or joints of different sizes. If creation of surface areas is a driving force in the design of cancellous bone, then CTS-type scaling would be favored. CTS scaling provides a far greater increase in surface area with body size than does CTG scaling, increasing as (size factor)$^{2.93}$ (Table 2); size factor is a linear dimension; hence, this is equivalent to scaling in proportion to volume or mass$^{0.97}$, or nearly in direct proportion to body mass. Metabolic rates, however, do not increase in direct proportion to body mass, but rather to (body mass)$^{0.75}$ (Kleiber, 1932; Schmidt-Nielsen, 1975; Calder, 1984). Exact CTS scaling would therefore not directly match the scaling of metabolic rate, but could accommodate the metabolic demands of increased size. With CTG scaling, trabecular surface area increases only in proportion to (size factor)$^{2.00}$ (Table 2) or (body mass)$^{0.67}$. It is possible, however, that metabolic requirements could drive the architecture of cancellous bone tissue even in the absence of a close match of scaling coefficients for trabecular surface area and metabolic rate; calcium metabolism may not scale in direct proportion to overall metabolic rate, and the proportion of trabecular surface active in remodeling may not be the same at all sizes. This issue clearly requires further study. Moreover, while available surface area is clearly an important determinant of bone remodeling, Haversian remodeling occurs deep within bony tissue, away from free surfaces. This remodeling can occur not only within compact cortical bone, but also in large,

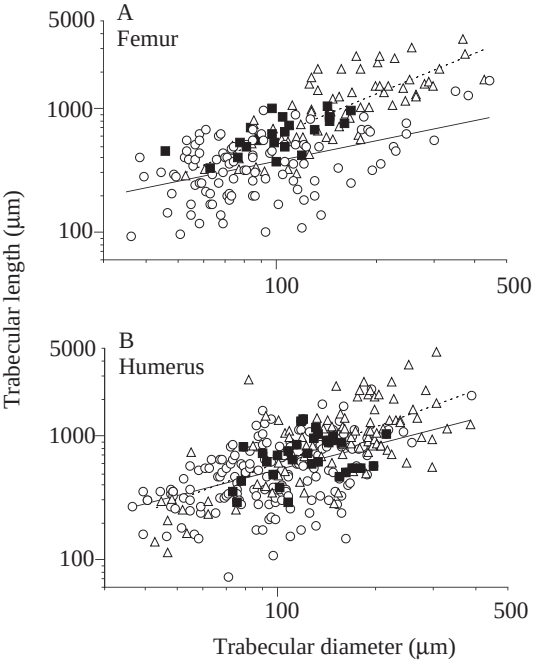

Fig. 7. Double-logarithmic plot of trabecular length in relation to trabecular diameter for bats and non-volant mammals with least-squares regression lines. Each point represents a separate trabecula. Bats are indicated as triangles and non-volant mammals as circles; highly terrestrial vampire bats are indicated as filled squares for comparison with other taxa. Solid lines indicate regression lines for bats, dashed lines for non-volant mammals.

vascularized trabeculae (Sato *et al.* 1986; Luzopone and Favia, 1990).

The relationship between the mechanical properties of cancellous bone and the surface area or volume of tissue may be more complex. The mechanical properties of synthetic, engineered cellular materials are dictated by their relative density, ρ^*/ρ_s, where ρ^* is the density of the cellular material or foam and ρ_s is the density of the material of which it is made (Gibson and Ashby, 1988). The volume fraction of supporting material, in this case the bony trabeculae, is the critical

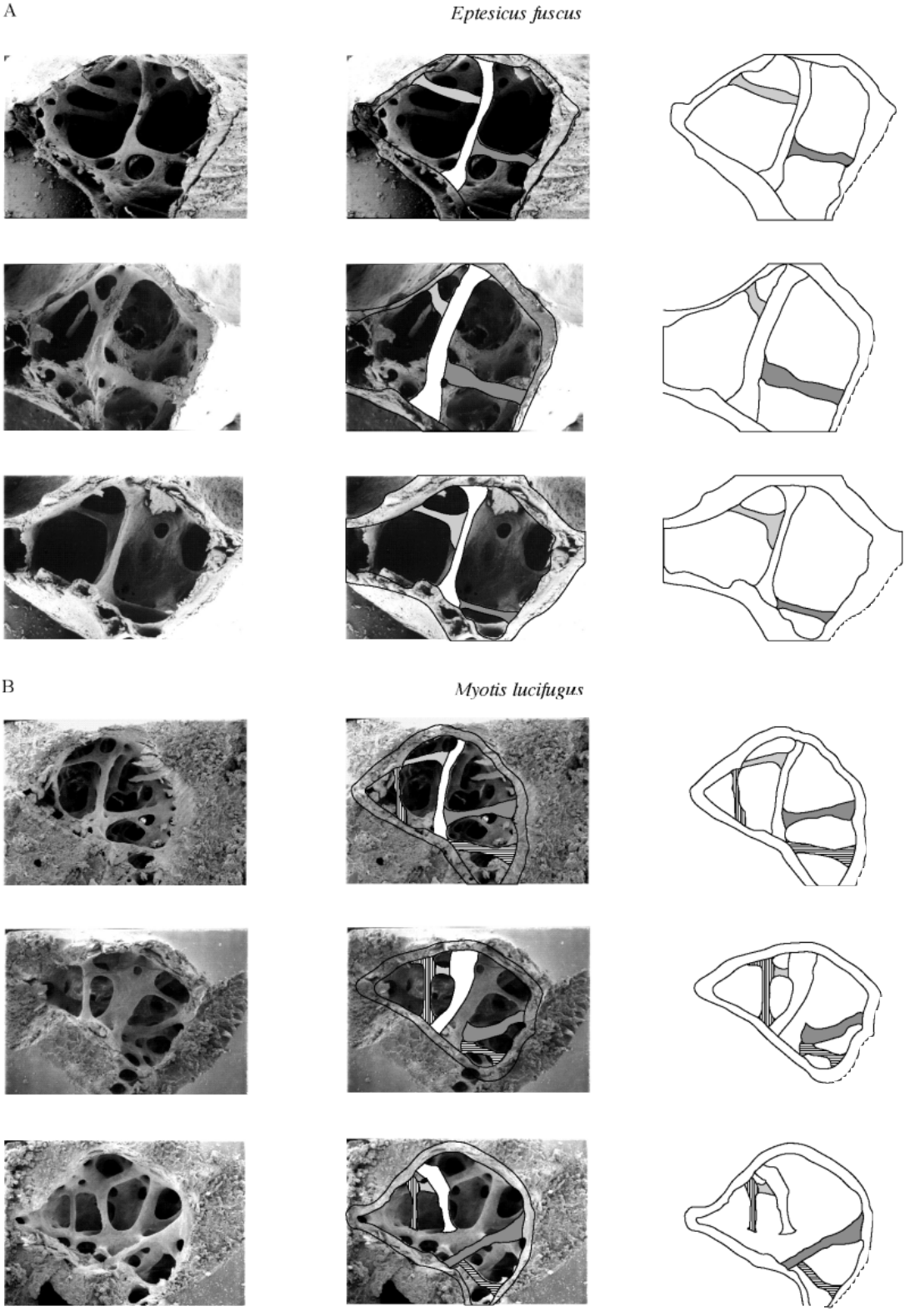

Fig. 8. Homology of trabecular elements within and between *Eptesicus fuscus* and *Myotis lucifugus*, members of distinct genera of vespertilionid bats. Each image represents a single standardized view of the cut inferior surface of the humeral head, looking proximally towards the joint surface along the bone shaft, towards the distal-most trabeculae. Scanning electron micrographs of three representative specimens appear in the left-hand column of both A and B. In the center column, outline tracings of individual trabeculae are superimposed on these images; homologous elements are coded with the same shading patterns and homologies appear to extend both within and between species. The right-hand column presents the outline drawings only of the cortical shell and homologous trabeculae

determinant of the strength and stiffness of cellular solids in general. Trabecular bone fits this model extremely well (Carter and Hayes, 1977; Gibson, 1985; Rice *et al.* 1988), with strength increasing approximately in proportion to the square of apparent density. However, if trabeculae scaled isometrically, as in the CTG model, trabecular bone density (trabecular bone volume/joint volume; Fig. 3D) would remain constant and relatively high with respect to CTS scaling. Thus, the tissue modulus would remain constant with increasing size and weight-bearing, as would tissue strength, in contrast to a typical cellular material. This suggests that CTG scaling would be mechanically advantageous. Density values in the two models are identical at the smallest size, but decrease precipitously for joints between 1.1 and 10 mm edge length for CTS scaling, rapidly declining to approximately 2.5 times less than the density of tissue under CTG scaling. If a low modulus is important for energy absorption in trabecular bone, then perhaps there could be some compensating benefit of a decreased modulus with increasing size for large body sizes.

Strength and modulus may, however, decrease with increasing surface area to volume ratio; Choi *et al.* (1990) and Martin (1991) have demonstrated that the modulus of cortical bone specimens decreases with increasing surface area to volume ratio and argue that high surface area to volume ratio may increase the likelihood of surface defects and their relative importance in determining mechanical failure. In the CTS model, the surface area to volume ratio is almost constant, while in the CTG model, this ratio decreases in direct proportion to animal size. As a consequence, at the largest size in our model, the surface area to volume ratio is 95 times greater for CTS scaling. Surface area to volume ratios are higher for CTS scaling at all sizes (Fig. 4A), and the ratio of CTS to CTG surface area to volume increases linearly with size (Fig. 4B). Thus, the frequency of surface defects is likely to be higher for the CTS model, and this disadvantage increases in severity with body size.

CTG scaling might also confer mechanical benefits directly from the increased volume of trabecular bone tissue, irrespective of the effects of density or surface area to volume ratio. The amount of tissue available for the distribution of loads as well as the greater cross-sectional area of the trabecular elements would be likely to reduce tissue stress and, hence, the accumulation of fatigue damage (Burr *et al.* 1985). Although the high surface area to volume ratios of CTS scaling provide surface area for the remodeling and repair of damaged tissues, it seems unlikely that this advantage could fully counter the mechanical disadvantages of CTS scaling.

The functional characteristics of trabecular bone must change with changing body size unless trabecular geometry or other phenomena are significantly altered with changing size. The ability of trabecular bone to meet simultaneously the need to regulate calcium levels and repair damaged tissue, on the one hand, and to maintain mechanical strength and stiffness, on the other, will change as surface area to volume ratio changes. It is a plausible hypothesis that trabeculae could maintain either constant size or isometric scaling and constant geometry, or some intermediate alternative. However, the two extremes produce dramatically different structural designs, particularly at large body sizes. The contrasts between the results of these distinct models suggest that the relative importance of surface area and volume in the functional performance of trabecular bone may exert a strong influence on the way in which trabecular dimensions scale. The negative allometry of trabecular dimensions inherent in the CTS model will produce disproportionately increasing surface area with increasing size. Isometry of trabecular dimensions, an intrinsic element of the CTG model, produces increasing volume of trabecular tissue with increasing size. The ratio of trabecular surface area to volume is also favored at large sizes by the scaling of the CTS model. Comparison of empirical allometric data with these contrasting models may be able to provide some suggestions for the critical design constraints on trabecular bone.

Predicting the allometry of trabecular dimensions

Design principles based on geometric scaling predict that forces experienced by the skeleton scale approximately in proportion to (body mass)$^{1.00}$, while the ability of structural elements to withstand axial forces depends on their cross-sectional area, proportional to (body mass)$^{0.67}$ (Alexander, 1971; Biewener, 1982; Calder, 1984; LaBarbera, 1989). Within mammals, whole bones appear to scale isometrically, showing little change in shape with increasing size [linear dimensions scale in close proportionality to (body mass)$^{0.33}$] (e.g. Alexander *et al.* 1979; Maloiy *et al.* 1979; Biewener, 1982; Jungers, 1985; Biknevicius, 1993; Steudel and Beattie, 1994). One reasonable null hypothesis for trabecular scaling is that trabeculae will scale isometrically as do whole bones. Alternatively, if trabeculae carry out their mechanical function by serving as a network of beams loaded primarily in axial tension or compression (Roesler, 1981; Currey, 1984; Lanyon, 1992*b*), structural design considerations predict that their cross-sectional areas should scale in a manner appropriate for accommodating joint forces. If joint loads scale in proportion to muscle forces, that is as (body mass)$^{0.74}$ (Biewener, 1989), then the cross-sectional area of trabeculae that bear those loads should also scale in proportion to (body mass)$^{0.74}$, and trabecular diameter should scale in proportion to mass$^{\geqslant 0.37}$ if the number of elements is constant. If joint forces scale in direct proportion to body mass, as has also been proposed (McMahon, 1977; Cavagna *et al.* 1977), the corresponding expectation for trabecular diameter would be scaling in proportion to mass$^{\geqslant 0.50}$. However, the relevant cross-sectional area could be provided either by a small number of large elements or by a large number of small elements, if the area over which the force is distributed is adequate. The scaling relationship of trabecular diameters could, therefore, be influenced by allometric shape changes in the elements. If trabeculae function as beams loaded in bending rather than axially (Gibson, 1985; Michel *et al.* 1993), then the stress developed within the element can be estimated from the standard equation for bending stress in a beam: $\sigma = My/I$, where σ is bending stress, M is the applied bending moment (the product of the body-mass-related load and the moment arm at which the bending force is applied, maximally the length of the trabecula), y is the distance from the beam's

neutral axis to its outermost surface (typically half the diameter), and I is the second moment of area of the beam's cross section, proportional to the fourth power of the diameter. To produce constant stress in trabeculae under bending with increasing body mass, assuming that the length of trabeculae scales isometrically and that applied force scales in proportion to mass, trabecular diameter would have to scale in proportion to mass$^{0.44}$.

If, however, trabecular bone functions as a cellular solid (*sensu* Gibson and Ashby, 1988), then it is the trabecular volume fraction that should scale in proportion to applied load, and specific predictions for diameter scaling will depend strongly on the length and number of trabeculae making up a given volume of tissue. Thus, it is important to note that the length and diameter scaling of individual trabeculae interface with the scaling of trabecular volume and density ultimately to produce tissue architecture. This implies that there may be a variety of ways for trabeculae to interconnect to one another such that varying numbers of trabeculae of the same size can be packed into the same total volume, depending on the nature and number of trabecula-to-trabecula and trabecula-to-cortical bone connections. In our theoretical models, we have imposed a regular geometry that only permits trabecula-to-trabecula connections at the corners of each cubic subunit; real trabecular architecture is more complex.

The total volume of trabecular bone in femoral and humeral heads, assessed by quantitative radiography, has been found to scale in direct proportion to body mass (Rafferty, 1996). Total trabecular tissue volume, V_t, is therefore proportional to ld^2n_t, where l is mean trabecular element length, d is mean element diameter, and n_t is the number of trabeculae. It follows that

$$\left(\frac{V_t}{ld^2} \right) \propto n_t \qquad (1)$$

and, if trabecular length and diameter scale isometrically, n_t will be constant and:

$$n_t \propto \frac{m^{1.00}}{m^{0.33}(m^{0.33})^2} = m^0 , \qquad (2)$$

where m is body mass.

However, trabeculae are not whole bones and appear not to have the same kind of individual identity as whole bones or other major organs. As nearly microscopic entities, one might predict that they should scale like other sub-organ-level structures. For example, red blood cells and the cross sections of skeletal muscle fibers are largely scale-independent (Munro, 1969; Altman and Dittmer, 1972). Trabecular length and diameter may also be scale-independent (proportional to m^0); if so, adequate function over a large range of body sizes could be achieved through changes in the density or number of trabeculae. In this scenario,

$$n_t \propto \frac{m^{1.00}}{m^{0.00}(m^{0.00})^2} = m^{1.00} , \qquad (3)$$

with n_t increasing in direct proportion to body mass.

Scaling of trabeculae: relationship between empirical results and models

Although trabeculae are macroscopic structures comprising many bone cells and their associated extracellular matrix, scaling of trabecular dimensions shows little size-dependence. Instead, humeral and femoral trabecular lengths and diameters scale negatively, unlike the whole bones of which they are a part (Table 5; Fig. 5). The negative allometry of trabecular dimensions we describe here, a pattern approaching the CTS model, implies that both the absolute and relative surface area of trabecular tissue are smaller in small than in large animals. This result is, to some extent, consistent with expectations based on the need to increase trabecular surface area in relation to metabolic rate, although the scaling of the CTS model does not match metabolic scaling precisely.

Although the relative size of trabeculae in small animals is much greater than in large ones, the mechanical consequences of such differences are unclear. The volume fraction and apparent density are the primary determinants of the mechanical properties of trabecular bone (Carter and Hayes, 1977; Gibson, 1985; Rice *et al.* 1988). Trabecular bone can vary in apparent density even within a single large joint, and large and small mammals show no systematic differences in trabecular apparent density. Trabecular volume fraction has been found to scale in proportion to (body mass)$^{1.00}$ in primates over a body size range of 3–90 kg (Rafferty, 1996). If this relationship holds for all mammals, one might infer that there are no systematic scale-related differences in the strength and stiffness of cancellous bone. This result is consistent with findings that locomotor loads are mitigated through postural and behavioral mechanisms in larger mammals to maintain constant locomotor stresses (Biewener, 1989). If the tissue that comprises trabecular bone has relatively uniform mechanical properties over a large body size range, and if networks of cancellous bone are able to withstand load in proportion to trabecular volume fraction rather than cross-sectional area, then the isometric scaling of trabecular volume fraction suggests that trabecular bone may modulate mechanical function by varying geometry and hence volume; this, in turn, would vary with varying body mass. However, it is not yet clear whether trabecular and compact material are mechanically similar (e.g. Hodgskinson and Currey, 1992; Rho *et al.* 1993), let alone whether there is regional or interspecific variation in the mechanical properties of trabecular material. Moreover, experimental work documents that the mechanical behavior of trabecular bone is strongly influenced by specimen size and geometry irrespective of mechanical properties of bone material (Keaveny *et al.* 1993). These size- and shape-dependent aspects of mechanical behavior could certainly influence the mechanics of trabecular bone *in situ* as well as in a testing apparatus.

Moreover, the mechanical behavior of trabecular bone is not determined solely by the volume fraction. Both the orientation of trabeculae relative to the direction of applied forces and the

number and orientations of interconnections among trabecular elements affect trabecular bone mechanics (Goldstein, 1987; Parfitt *et al.* 1987; Mosekilde, 1990; Parfitt, 1992; Keaveny and Hayes, 1993). The observed negative allometry indicates that trabeculae of larger animals have an increased surface area. This surface area patterning consequence may relate to differences among animals of varying size in patterns of interconnection among trabecular elements. Our results confirm that, in at least one respect, these patterns change fundamentally with body size. In large animals, the vast majority of trabeculae connect directly to one another, while only a very small proportion of elements connect to the compact bone shell supporting the overlying articular cartilage. In contrast, in small animals, most or all trabeculae span the entire epiphysis and connect directly to subchondral and epiphyseal compact bone, with relatively few interconnections among trabeculae (Fig. 8). Future studies may uncover key differences in the functionality of joint mechanics arising from these structural variations. Given that bone in small animals is often used to model the human skeleton, and that both the earliest known and the vast majority of extant and extinct mammals are less than 1 kg in mass, it is critical to pursue a better understanding of the ramifications of this pattern of structural design.

The comparative biology of trabecular architecture: do flying and non-flying taxa differ?

The trabecular morphology of bats does not differ from that of their non-volant relatives in a systematic fashion that is readily interpretable with respect to their distinct manner of limb usage (Figs 5, 6). In the femoral head, although the slope of the bat trabecular dimension regressions is far steeper than that of the remainder of the sample, the elevations of the two regressions do not differ, i.e. the trabeculae of bats are within the size range of non-volant mammals. For the humerus, trabecular dimensions among the two locomotor groups are, again, broadly overlapping with steeper slopes in bats and with some tendency for bat trabeculae to be somewhat longer but not wider than those of quadrupeds and bipeds. The length of the entire humerus is also significantly greater in bats than in non-volant mammals. However, this increased bone length does not account for the increased trabecular length; when we recalculate regressions of trabecular length with respect to humerus length rather than body mass, bat humeral trabeculae remain significantly longer.

The slope differences among bats and non-volant mammals could lead to considerable divergence in trabecular dimensions at large body sizes. However, the 700 g bats at the extreme range of our bat sample (*Pteropus poliocephalus*) approach the maximum body mass for bats (*Pteropus giganteus*, approximately 1500 g; Silva and Downing, 1995). The steep slope of the bat regression line may therefore be a reflection of a pattern that is discernible within the non-volant sample as well: the relationships between log(trabecular dimensions) and log(body mass) are reasonably well fitted by a linear regression, but there is some curvilinearity in the relationship as well, with a tendency for moderately sized animals to possess somewhat larger trabeculae than either their larger or smaller relatives.

The similarity in trabecular dimensions of the bat humerus and femur occurs despite the gross differences in joint loading that must be experienced by the fore- *versus* hindlimbs in bats. Bat forelimbs accommodate the large forces generated during powered flight, and although shoulder-joint reaction forces or epiphyseal strains have never been measured directly, there are indications that the stresses in the bat shoulder during both the down- and upstroke are considerable (Rayner, 1987; P. Watts, personal communication). The hindlimbs, despite their anatomical connection to the wing membrane, probably experience only very small forces during flight and little force during roosting or climbing behaviors. The most likely exceptions to this patterns are the vampire bats, characterized by vigorous terrestrial and/or arboreal jumping and climbing (Altenbach, 1979). These three species experience considerably larger hindlimb forces than do their relatives, probably many times larger in most cases. Yet, the morphology of the trabecular bone of both the femoral and humeral head of vampire bats is indistinguishable from that of the other bats. Thus, we find no support for the hypothesis that differences in limb loading, either in intensity or in frequency, can produce differences in structure of individual trabeculae. Although it is possible that differences between femora and humeri or between vampires and their non-terrestrial relatives remain to be found in more detailed study of trabecular density or orientation, visual inspection of our specimens provides no indication that this is likely.

Topology and homology of trabeculae in small mammals

The total number of trabeculae in a joint, n_t, is not necessarily constant, but scales in proportion to V_t/ld^2. We found that trabecular number is size-dependent, scaling in proportion to $m^{0.62–0.87}$, depending on whether one considers the femur or humerus and the entire sample or non-volant mammals alone, assuming that volume scales in proportion to mass. A key consequence of this pattern is that small animals have extremely reduced trabecular complexity, with fewer than 20 trabeculae in a given joint, compared with thousands or millions in the larger joints of large mammals. The simplified trabecular architecture of small mammals allows us to make, for the first time, direct comparisons of element topology among individuals of a given species. We found that particular trabeculae can be directly homologized among different individuals of a given species (Fig. 8). Although a given trabecula varies among individuals in details of morphology and absolute position, it can be repeatably and reliably identified as a topologically distinct entity in each specimen. Furthermore, these homologies can extend among species (Fig. 8).

The presence of topological homology suggests that there

may be fundamental constraints on the construction of trabecular tissue. This unexpected similarity in positioning of individual elements both within and among species could arise by at least two alternative mechanisms. First, genetic information may directly specify the development of each element, as it does, to a certain extent, the ontogeny of whole bones. As in whole-bone maturation, the mechanical environment imposed on the growing trabecular tissue may then secondarily influence the ultimate size, shape and details of placement of each element, but only within a limited range of plasticity. Alternatively, the architecture of trabecular tissue, including element number and placement, may be largely epigenetic (e.g. Fyhrie and Carter, 1986; Whalen *et al.* 1988; Wong and Carter, 1990; Carter *et al.* 1991). Basic genetic information might encode only that a given region will form trabecular tissue. The details of the structural patterning in the tissue would, from this perspective, arise in response to some function of the magnitude, direction and/or frequency of applied loads. The similarities observed here intra- and interspecifically would then be interpretable as arising from similarity in the mechanical signals received by the phenotypically plastic tissue. In this framework, considerable similarity in limb usage patterns among individuals within species must exist to account for the within-species homologies observed in this study. Distinguishing among these different hypotheses is not a trivial problem, and, to date, there are insufficient data to reject or to support strongly either view.

Appendix 1. *Formulae for parameters of the CTS and CTG models*

Constant trabecular size: (CTS) model

n_t	Total number of trabeculae	$3n(n+1)^2$
A_t	Total trabecular surface area	$3n(n+1)^2(4la)+24a^2+24a^2(n-1)+6a^2(n-1)^2$
A_j	Total joint surface area	$6(nl+na+a)^2$
$\frac{A_t}{A_j}$	$\frac{\text{Total trabecular surface area}}{\text{Total joint surface area}}$	$\frac{3n(n+1)^2(4la)+24a^2+24a^2(n-1)+6a^2(n-1)^2}{6(nl+na+a)^2}$
V_t	Total trabecular volume	$3n(n+1)^2(la^2)+a^3(n+1)^3$
V_j	Total joint volume	$(nl+na+a)^3$
$\frac{V_t}{V_j}$	$\frac{\text{Total trabecular volume}}{\text{Total joint volume}}$	$\frac{3n(n+1)^2(la^2)+a^3(n+1)^3}{(nl+na+a)^3}$
$\frac{A_t}{V_t}$	$\frac{\text{Total trabecular surface area}}{\text{Total trabecular volume}}$	$\frac{3n(n+1)^2(4la)+24a^2+24a^2(n-1)+6a^2(n-1)^2}{3n(n+1)^2(la^2)+a^3(n+1)^3}$

Constant trabecular geometry: (CTG) model

k	Adjusted size factor	$\frac{(nl+a(n+1))}{(2a+l)}$
A_t	Total trabecular surface area	$24a(2l+a)\left(\frac{nl+na+a}{2a+l}\right)^2$
A_j	Total joint surface area	$6(nl+na+a)^2$
$\frac{A_t}{A_j}$	$\frac{\text{Total trabecular surface area}}{\text{Total joint surface area}}$	$\frac{24a(2l+a)\left(\frac{nl+na+a}{2a+l}\right)^2}{6(nl+na+a)^2}$
V_t	Total trabecular volume	$4a^2(3l+2a)\left(\frac{nl+na+a}{2a+l}\right)^3$
V_j	Total joint volume	$(nl+na+a)^3$
$\frac{V_t}{V_j}$	$\frac{\text{Total trabecular volume}}{\text{Total joint volume}}$	$\frac{4a^2(3l+2a)\left(\frac{nl+na+a}{2a+l}\right)^3}{(nl+na+a)^3}$
$\frac{A_t}{V_t}$	$\frac{\text{Total trabecular surface area}}{\text{Total trabecular volume}}$	$\frac{24a(2l+a)\left(\frac{nl+na+a}{2a+l}\right)^2}{4a^2(3l+2a)\left(\frac{nl+na+a}{2a+l}\right)^3}$

n is the case or iteration number and indicates the number of subunits along one edge for the CTS model.
The trabecular framework in each cube consists of struts and interconnetion cubes.
l is strut length, and a is the diameter of the strut and the length of each edge of the interconnection cubes (see Fig. 1).

This study was carried out with the support of grants from the Whitaker Foundation and the National Science Foundation (NSF-IBN-9119143) to S.M.S. Specimens were generously supplied by Andrew Biewener, Jennifer Gray Chickering, Patricia Freeman, Tom Kunz, Winston Lancaster, Deborah Morris, Jim Ryan, Jim Simmons and Nancy Simmons and include material from the collections of the American Museum of Natural History. Sandy Kunz provided scanning electron microscope expertise and guidance, and Don Chickering assisted in the production of photomicrographs. Dave Carrier read drafts of an earlier version of this manuscript, and we have benefited greatly from his insight. We are also thankful for the very helpful suggestions of two anonymous reviewers; their critiques substantially improved this paper.

References

ALEXANDER, R. MCN. (1971). *Size and Shape*. London: Edward Arnold.

ALEXANDER, R., MCN., JAYES, A. S., MALOIY, G. M. O. AND WATHUTA, E. M. (1979). Allometry of the limb bones of mammals from shrews (*Sorex*) to elephants (*Loxodonta*). *J. Zool., Lond.* **89**, 305–314.

ALTENBACH, S. J. (1979). Locomotor morphology of the vampire bat, *Desmodus rotundus*. *Spec. Pub. Am. Soc. Mammal.* **6**, 1–133.

ALTMAN, P. L. AND DITTMER, D. S. (1972). *Biology Data Book.* Bethesda: Federation of American Societies for Experimental Biology.

BEAUPRÉ, G. S., ORR, T. E. AND CARTER, D. R. (1990). An approach for time-dependent bone modeling and remodeling – theoretical development. *J. orthop. Res.* **8**, 651–661.

BIEWENER, A. A. (1982). Bone strength in small mammals and bipedal birds: do safety factors change with body size? *J. exp. Biol.* **98**, 289–301.

BIEWENER, A. A. (1983). Allometry of quadrupedal locomotion: the scaling of duty factor, bone curvature and limb orientation to body size. *J. exp. Biol.* **105**, 147–171.

BIEWENER, A. A. (1989). Scaling body support in mammals: limb posture and muscle mechanics. *Science* **245**, 45–48.

BIKNEVICIUS, A. R. (1993). Biomechanical scaling of limb bones and differential limb use in caviomorph rodents. *J. Mammal.* **74**, 95–107.

BURR, D. B., MARTIN, R. B., SCHAFFLER, M. B. AND RADIN, E. L. (1985). Bone remodeling in response to *in vivo* fatigue microdamage. *J. Biomech.* **18**, 189–200.

CALDER III, W. A. (1984). *Size, Function and Life History.* Cambridge, MA: Harvard University Press.

CARTER, D. R. (1987). Mechanical loading history and skeletal biology. *J. Biomech.* **20**, 1095–1109.

CARTER, D. R., FYHRIE, D. P. AND WHALEN, R. T. (1987). Trabecular bone density and loading history: regulation of connective tissue biology by mechanical energy. *J. Biomech.* **20**, 785–794.

CARTER, D. R. AND HAYES, W. C. (1977). The compressive behavior of bone as a 2-phase porous structure. *J. Bone Jt Surg.* **59**A, 954–962.

CARTER, D. R., WONG, M. AND ORR, T. E. (1991). Musculoskeletal ontogeny, phylogeny and functional adaptation. *J. Biomech.* **4**, 3–16.

CAVAGNA, G. A., HEGLUND, N. C. AND TAYLOR, C. T. (1977). Mechanical work in terrestrial locomotion: two basic mechanisms for minimizing energy expenditure. *Am. J. Physiol.* **233**, 243–261.

CHOI, K., KUHN, J. L., CIARELLI, M. J. AND GOLDSTEIN, S. A. (1990). The elastic moduli of human subchondral, trabecular and cortical bone tissue and the size-dependency of cortical bone modulus. *J. Biomech.* **23**, 1103–1113.

CURREY, J. D. (1984). *The Mechanical Adaptations of Bones*. Princeton, NJ: Princeton University Press.

ECONOMOS, A. C. (1983). Elastic and/or geometric similarity in mammalian design? *J. theor. Biol.* **103**, 167–172.

FYHRIE, D. P. AND CARTER, D. R. (1986). A unifying principle relating stress to trabecular bone morphology. *J. orthop. Res.* **4**, 304–317.

GIBSON, L. J. (1985). The mechanical behavior of cancellous bone. *J. Biomech.* **18**, 317–328.

GIBSON, L. J. AND ASHBY, M. F. (1988). *Cellular Solids: Structure and Properties*. Oxford: Pergamon Press.

GOLDSTEIN, S. A. (1987). The mechanical properties of trabecular bone: dependence on anatomic location and function. *J. Biomech.* **20**, 1055–1061.

GREEN, H. L. H. H. (1934). A rapid method of preparing clean bone specimens from fresh or fixed material. *Anat. Rec.* **61**, 1–3.

HAYES, W. C. AND SNYDER, B. (1982). Stress–morphology relationships in the trabecular bone of the patella. In *Finite Elements in Biomechanics* (ed. R. H. Gallagher, B. R. Simon, P. C. Johnson and J. F. Gross), pp. 223–268. New York: John Wiley and Sons, Ltd.

HODGKINSON, R. AND CURREY, J. D. (1992). Young's modulus, density and material properties in cancellous bone over a large density range. *J. Mat. Sci. Mat. Med.* **3**, 377–381.

JEE, W. S. S., MORI, S., LI, X. AND CHAN, S. (1990). Prostaglandin E_2 enhances cortical bone mass and activates intracortical bone remodeling in intact and ovariectomized female rats. *Bone* **11**, 253–266.

JEE, W. S. S., UENO, K., DENG, Y. P. AND WOODBURY, D. M. (1985). The effects of prostaglandin E_2 in growing rats: increased metaphyseal hard tissue and cortico-endosteal bone formation. *Calcif. Tissue Int.* **37**, 148–157.

JUNGERS, W. L. (1985). *Size and Scaling in Primate Biology.* New York: Plenum Press.

KAPLAN, F. S., HAYES, W. C., KEAVENY, T. M. A. B., EINHORN, T. A. AND IANOTTI, J. P. (1994). Form and function of bone. In *Orthopedic Basic Science* (ed. S. R. Simon), pp. 127–184. American Academy of Orthopedic Surgeons.

KEAVENY, T. M., BORCHERS, R. E., GIBSON, L. J. AND HAYES, W. C. (1993). Trabecular bone modulus and strength depend on specimen geometry. *J. Biomech.* **26**, 991–1000.

KEAVENY, T. M. AND HAYES, W. C. (1993). Mechanical properties of cortical and trabecular bone. In *Bone*, vol. 7, *Bone Growth – B* (ed. B. K. Hall), pp. 285–344. Boca Raton: CRC Press.

KLEIBER, M. (1932). Body size and metabolism. *Hilgardia* **6**, 315–353.

KU, J. L., GOLDSTEIN, S. A., CHOI, K. W., LONDON, M., HERZIG, M. A. AND MATTHEWS, L. S. (1987). The mechanical properties of single trabeculae. *Trans. 33rd orthop. Res. Soc.* **12**, 48.

LABARBERA, M. (1989). Analyzing body size as factor in ecology and evolution. *A. Rev. ecol. Syst.* **20**, 97–118.

LANYON, L. E. (1974). Experimental support for the trajectorial theory of bone structure. *J. Bone Jt Surg.* **56**B, 160–166.

LANYON, L. E. (1992*a*). Osteocytes, strain detection, bone modeling and remodeling. *Calc. Tissue Int.* **53**, S103–S107.

LANYON, L. E. (1992*b*). The success and failure of the adaptive response to functional load-bearing in averting bone fracture. *Bone* **13**, S17–S21.

LANYON, L. E. AND RUBIN, C. T. (1985). Functional adaptation in skeletal structures In *Functional Vertebrate Morphology* (ed. M. Hildebrand, D. Bramble, K. F. Liem and D. B. Wake), pp. 1–25. Cambridge, MA: Harvard University Press.

LUZOPONE, E. AND FAVIA, A. (1990). The structure of the trabeculae of cancellous bone. *Calcif. Tissue Int.* **46**, 367–372.

MALOIY, G. M. O., ALEXANDER, R., MCN., NJAU, R. AND JAYES, A. S. (1979). Allometry of the legs of running birds. *J. Zool., Lond.* **187**, 161–167.

MARTIN, R. B. (1991). Determinants of the mechanical properties of bones. *J. Biomech.* **24**S, 79–88.

MCMAHON, T. A. (1977). Scaling quadrupedal galloping: frequencies, stresses and joint angles. In *Scale Effects in Animal Locomotio*. (ed. T. J. Pedley), pp. 143–151. Cambridge: Cambridge University Press.

MENTE, P. L. AND LEWIS, J. (1989). Experimental method for the measurement of the elastic modulus of trabecular bone tissue. *J. orthop. Res.* **7**, 456–461.

MEYER, G. H. (1867). Die Architektur der Spongiosa. *Arch. Anat. Physiol. Wiss. Med.* **34**, 615-628.

MICHEL, M. C., GUO, X.-D. E., GIBSON, L. J., MCMAHON, T. A. AND HAYES, W. C. (1993). Compressive fatigue behavior of bovine trabecular bone. *J. Biomech.* **4/5**, 453–463.

MILLER, M. A., OMURA, T. H. AND MILLER, S. C. (1989). Increased cancellous bone remodeling during lactation in beagles. *Bone* **10**, 279–285.

MORI, S., JEE, W. S. S., LI, X., CHAN, S. AND KIMMEL, D. B. (1990). Effects of prostaglandin E_2 on production of new cancellous bone in the axial skeleton of ovariectomized rats. *Bone* **11**, 103–113.

MOSEKILDE, L. (1990). Consequences of the remodeling process for vertebral trabecular bone structure: a scanning electron microscope study (uncoupling of unloaded structures). *Bone Min.* **10**, 13–35.

MUIR, B. S. AND HUGHES, G. M. (1969). Gill dimensions for three species of tunny. *J. exp. Biol.* **51**, 271–285.

MUNRO, H. N. (1969). Evolution of protein metabolism in mammals. In *Mammalian Protein Metabolism* (ed. H. N. Munro), pp. 133–182. New York: Academic Press.

NOWAK, R. M. (1991). *Walker's Mammals of the World*. 5th edition. Baltimore: Johns Hopkins University Press.

PARFITT, A. M. (1983). The physiological and clinical significance of bone histomorphometric data. In *Bone Histomorphometry: Techniques and Interpretations* (ed. R. Recker), pp. 143–223. Boca Raton, FL: CRC Press.

PARFITT, A. M. (1988). Bone histomorphometry: standardization of nomenclature, symbols and units. *J. Bone Min. Res.* **2**, 595–610.

PARFITT, A. M. (1992). The physiologic and pathogenic significance of bone histomorphometric data. In *Disorders of Bone and Mineral Metabolism* (ed. F. L. Coe and M. J. Favus), pp. 475–489. New York: Raven Press.

PARFITT, A. M., KLEEREKOPER, M. AND VILLANUEVA, A. R. (1987). Increased bone age: mechanisms and consequences. In *Osteoporosis* (ed. C. J. C. Christiansen and B. J. Riis), pp. 301–308. Copenhagen: Osteopress APS.

PRANGE, H. D., ANDERSON, J. F. AND RAHN, H. (1979). Scaling of skeletal mass to body mass in birds and mammals. *Am. Nat.* **113**, 103–122.

RADIN, E. L. (1982). Mechanical factors in the causation of osteoarthritis. *Rheumatology* **7**, 46–52.

RADIN, E. L., PARKER, H. G., PUGH, J. W., STEINBERG, R. S., PAUL, I. L. AND ROSE, R. M. (1973). Response of joints to impact loading. III. Relationship between trabecular microfractures and cartilage degeneration. *J. Biomech.* **6**, 51–57.

RADIN, E. L., PAUL, I. L. AND LOWY, M. (1970). A comparison of the dynamic force transmitting properties of subchondral bone and articular cartilage. *J. Bone Jt Surg*. **52**A, 444–456.

RAFFERTY, K. (1996). Joint design in primates: external and subarticular properties in relation to body size and locomotor behavior. PhD dissertation, Johns Hopkins University, Baltimore, MD.

RAYNER, J. M. V. (1987). The mechanics of flapping flight in bats. In *Recent Advances in the Study of Bats* (ed. M. B. Fenton, P. Racey and J. V. M. Rayner), pp. 23–42. Cambridge: Cambridge University Press.

RHO, J. Y., ASHMAN, R. B. AND TURNER, C. H. (1993). Young's modulus of trabecular and cortical bone material: ultrasonic and microtensile measurements. *J. Biomech.* **26**, 111–119.

RICE, J. C., COWIN, S. C. AND BOWMAN, J. A. (1988). On the dependency of the elasticity and strength of cancellous bone on apparent density. *J. Biomech.* **21**, 155–168.

ROESLER, H. (1981). Some historical remarks on the theory of cancellous bone structure (Wolff's Law). In *Mechanical Properties of Bone* (ed. S. C. Cowin), AMD, vol. 45, pp. 27–42. New York: ASME Publications.

SATO, K., WAKAMATSU, E., SATO, T., HONMA, T., KOTAKE, H. AND BYERS, P. (1986). Histomorphometric study of trabecular channels in normal iliac bone. *Calcif. Tissue Int.* **39**, 2–7.

SCHMIDT-NIELSEN, K. (1975). Scaling in biology: the consequences of size. *J. exp. Zool.* **194**, 287–308.

SCHUTT, W. A., JR, HERMANSON, J. W., CULLINANE, D. M., CHANG, Y. H., ALTENBACH, J. S., MURADALI, F. AND BERTRAM, J. E. A. (1997). The dynamics of flight-initiating jumps in the common vampire bat *Desmodus rotundus*. *J. exp. Biol.* **200**, 3003–3012.

SILVA, M. AND DOWNING, J. A. (1995). *Handbook of Mammalian Body Masses*. Boca Raton, FL: CRC Press.

STEUDEL, K. AND BEATTIE, J. (1994). Scaling of cursoriality in mammals. *J. Morph.* **217**, 55–63.

SWARTZ, S. M., BENNETT, M. B. AND CARRIER, D. R. (1992). Wing bone stresses in free flying bats and the evolution of skeletal design for flight. *Nature* **359**, 726–729.

TSUTAKAWA, R. K. AND HEWETT, J. E. (1977). Quick test for comparing two populations with bivariate data. *Biometrika* **33**, 215–219.

VAUGHAN, T. A. (1959). Functional morphology of three bats: *Eumops, Myotis, Macrotus. Univ. Kansas Publ. Mus. nat. Hist.* **12**, 1–153.

WAINWRIGHT, S. A., BIGGS, W. D., CURREY, J. D. AND GOSLINE, J. M. (1976). *Mechanical Design in Organisms*. London: Edward Arnold.

WARD, S. C. AND SUSSMAN, R. W. (1979). Correlates between locomotor anatomy and behavior in two sympatric species of *Lemur*. *Am. J. phys. Anthrop.* **50**, 575–590.

WHALEN, R. T., CARTER, D. R. AND STEELE, C. R. (1988). Influence of physical activity on the regulation of bone density. *J. Biomech.* **21**, 825–837.

WHITEHOUSE, W. J. (1974). The quantitative morphology of anisotropic trabecular bone. *J. Microsc.* **101**, 153–168.

WHITEHOUSE, W. J. (1975). Scanning electron micrographs of cancellous bone from the human sternum. *J. Path.* **116**, 213–224.

WHITEHOUSE, W. J. AND DYSON, E. D. (1974). Scanning electron microscope studies of trabecular bone in the proximal end of the human femur. *J. Anat.* **118**, 417–444.

WOLFE, J. D. (1869). Über die Bedeutung der Architektur der spongiösen Substanz. **Zentralbl. Med. Wiss**. **VI**, 223–234.

WONG, M. AND CARTER, D. R. (1990). A theoretical model of endochondral ossification and bone architectural construction in long bone ontogeny. *Anat. Embryol.* **181**, 523–532.